International Journal of GEOMATE, Oct., 2022, Vol.23, Issue 98, pp.1-9
ISSN: 2186-2982 (P), 2186-2990 (O), Japan, DOI: https://doi.org/10.21660/2022.98.3447
Geotechnique, Construction Materials and Environment

NUMERICAL SIMULATION OF WAVE OVERTOPPING OF A VERTICAL POROUS DETACHED BREAKWATER

*Van Nghi Vu[1] and Van Khoi Pham[2]

[1]Institute of Civil Engineering, Ho Chi Minh City University of Transport, Vietnam; [2] Faculty of Civil Engineering, Vietnam Maritime University, Vietnam

*Corresponding Author, Received: 5 May 2022, Revised: 3 Aug. 2022, Accepted: 09 Sept. 2022

ABSTRACT: Various types of vertical porous detached breakwaters are being built to reduce the impact of wave pressure on sea dikes as well as avoid rapid, severe erosion along the coastline of the lower Mekong Delta area. Waves can both pass through the porous breakwater and over the top of the structure (overtopping). The effectiveness of porous structures varies because it depends on the crest freeboard height, breakwater width, and porosity. However, the effectiveness of this type of porous detached breakwater has yet to be proven. This paper evaluates the effectiveness of this type of breakwater by introducing a numerical model based on the Navier – Stokes equations applied to the porous media. The numerical model is applied to simulate solitary waves interacting with the porous structures for various cases. The numerical results show that when the crest freeboard is low (low-crested porous breakwater), the breakwater width and the porosity of the breakwater do not significantly affect the wave height behind the breakwater. The wave reduction effect is greatly increased with the increase of the crest height due to submerged breakwater and overtopping waves. The breakwater schematization is tested to show the porous breakwater effectiveness in reducing wave energy.

Keywords: Vertical porous detached breakwater; Numerical model; Overtopping; Navier – Stokes equations; Mekong Delta.

1. INTRODUCTION

Various numerical models are developed to simulate water waves interacting with porous structures or propagating inside porous media. Each model has its characteristics. The model applying extended Boussinesq equations saves time and gives good accuracy in simulating waves interacting with porous structures [1–6]. Nonlinear shallow water equations with hydrostatic pressure distribution have been widely used to simulate waves interacting with porous structures [7,8]. Recently, the Navier-Stokes equations have been applied to develop numerical models for waves in porous media [9–11]. Although this type of model is time-consuming, since it is a three-dimensional model, its accuracy is very good. Furthermore, the Navier-Stokes model has advantages in simulating three-dimensional phenomena such as diffraction, and refraction [10]. However, few studies apply this model in simulating overtopping waves of vertical porous breakwaters.

In recent years, several types of porous detached breakwaters have been deployed along the lower Mekong Delta coastal zone in Vietnam [12]. These detached breakwaters are placed about 100-200 m away from the coastline. The purpose of these detached structures is the reduction of wave impacts on the sea dike system- built a long time ago- which causes sediment accretion in the area between the breakwater and the sea dike, to plant mangrove forests. These mangrove forests are good for dissipating wave energy from storm surges, tidal flows, and result in the sediment accretion inside the forests [13,14]. Several different types of the porous detached breakwater are being built in the Mekong Delta area, such as hollow breakwaters, bamboo breakwaters, and vertical porous breakwaters filled with rocks. The first two types of breakwaters were introduced in some recent studies to show their advantages in reducing wave energy [5,11,15–18]. However, there are not many studies investigating the effectiveness of the third type of breakwater.

An analytical solution of wave interaction with a vertical porous structure was derived based on the matched Eigenfunction expansion method [19]. When waves interact with porous structures, the reflection, transmission, and energy loss coefficients are determined. However, the nonlinear energy dissipation was not considered because the fluid was assumed to be non-cohesive. Experiments were conducted to predict the transformation of waves passing through a double-row pile breakwater, which is similar to the vertical porous breakwater [20]. Figure 1 shows vertical porous breakwaters, which have been built recently along the coasts of the Vietnamese Mekong Delta [21] and Dongying City in China [19].

This type of vertical porous detached breakwater filled with rocks has been built in several pilot projects and gives good effectiveness in reducing wave forces impacting the sea dike system. Also, it increases the sediment deposition for mangrove development [12]. This paper evaluates the wave dissipation efficiency of this structure with various cases of breakwater widths, crest heights, porosities, and incident wave heights.

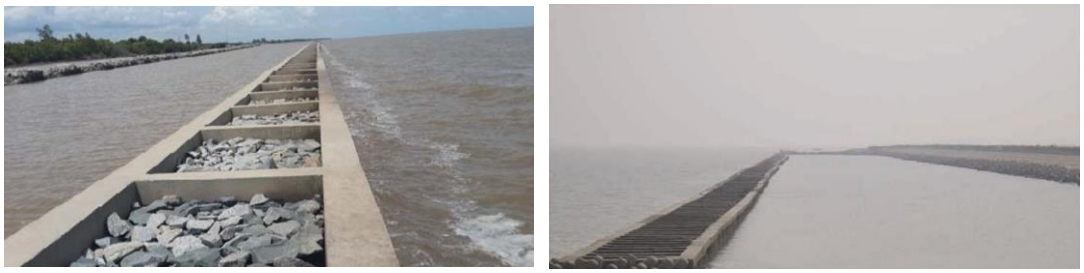

a) b)

Fig.1 Vertical porous detached breakwaters: a) along the west coast of Ca Mau province, Vietnam [21], b) along the coast of Dongying City, China [19].

In this study, a numerical model based on the Navier-Stokes equations is applied to study the waves overtopping of a porous breakwater protecting a coastal area in Southwest Vietnam, known as the Mekong Delta. The second section of this study introduces a numerical porous media model employing the turbulence model and a solitary wave boundary condition. The next section shows the stable propagation of the solitary wave which will be applied as an initial condition for the simulation of waves interaction with vertical porous detached breakwaters. By investigating various cases of breakwater configurations and porosity characteristics, the effectiveness of wave energy dissipation of the porous detached breakwater is analyzed and evaluated. The last section gives some concluding remarks.

2. MODEL DESCRIPTION

2.1 The Governing Equations for Water in Porous Media

By applying the framework of Navier-Stokes equations, the continuity and momentum equations in porous media [22,23] are given by

$$\nabla\cdot\left(A\mathbf{u}\right)=0 \tag{1}$$

$$\frac{\partial\mathbf{u}}{\partial t}+\frac{1}{V_F}\nabla\cdot(A\mathbf{u}\mathbf{u})=-\frac{1}{\rho}\nabla\cdot p+G+f_v-f_p \tag{2}$$

where $\nabla=\left(\partial/\partial x,\partial/\partial y,\partial/\partial z\right)$ is the gradient operator, $\mathbf{u}=\left(u,v,w\right)$ is the flow velocity in the x-, y-, z- direction; ρ is the water density; p is the pressure; G is the body acceleration; f_v is the viscous acceleration; and f_p is the flow losses in porous media. In this model, the geometry of porous media is captured by a grid which is separated into two parts. The first part captures the interface of the object (water) and the second one captures the filled part of the object (porous media). By defining the open volume fraction in the grid, the water and porous volumes are recognized in the grid based on the object parameters. Then, the fractional volume method is introduced to compute the mass and momentum equations in one unit cell. Here, A is the area fraction for the water in the mesh of a Cartesian coordinate system and V_F is the volume fraction for water.

By employing the famous switching technique of the volume of fluid (VOF) method [24], the free surface transportation equation between water and air is defined as

$$\frac{\partial V_{\mathrm{w}}}{\partial t}+\frac{1}{V_{\mathrm{F}}}\nabla\cdot\left(V_{\mathrm{w}}A\mathbf{u}\right)=0 \tag{3}$$

where V_{w} is the water volume fraction in the cell of a free surface and V_{w} = 0, 0 < V_{w} < 1 and V_{w} = 1 control the different phases of air, interface, and water, respectively.

The viscous acceleration vector, f_v, in three directions of Cartesian coordinate [23] can be written as:

(2)

$$\rho V_F f_{vx}=w_{sx}-\left[\frac{\partial}{\partial x}\left(A_x\tau_{xx}\right)+\frac{\partial}{\partial y}\left(A_y\tau_{xy}\right)+\frac{\partial}{\partial z}\left(A_z\tau_{xz}\right)\right] \tag{4}$$

$$\rho V_F f_{vy}=w_{sy}-\left[\frac{\partial}{\partial x}\left(A_x\tau_{yx}\right)+\frac{\partial}{\partial y}\left(A_y\tau_{yy}\right)+\frac{\partial}{\partial z}\left(A_z\tau_{yz}\right)\right] \tag{5}$$

$$\rho V_F f_{vz} = w_{sz} - \left[\frac{\partial}{\partial x}\left(A_x \tau_{zx}\right) + \frac{\partial}{\partial y}\left(A_y \tau_{zy}\right) + \frac{\partial}{\partial z}\left(A_z \tau_{zz}\right) \right] \quad (6)$$

where $w_{si(i=x,y,z)}$ is the wall-shear stress and τ is the shear stress term.

The flow losses in the porous media are derived using Forchheimer saturated drag [25] as:

$$f_p = F_D \frac{\mathbf{u}}{\lambda} \quad (7)$$

where λ is the porosity of the media, F_D is the Forchheimer saturated drag including the linear and non-linear terms as:

$$F_D = \alpha_l \frac{\mu}{\rho}\left(\frac{1-\lambda}{\lambda}\right)^2 + \alpha_t \frac{1-\lambda}{\lambda}\frac{|\mathbf{u}|}{\lambda} \quad (8)$$

In Eq. (8), α_l and α_t are coefficients that represent the laminar and turbulent flow resistances, respectively.

The turbulence model is applied for solving the dynamic viscosity μ using $k-\varepsilon$, giving the two equations [26,27]:

$$\frac{\partial k}{\partial t} + \frac{1}{V_F}\left(uA_x\frac{\partial k}{\partial x} + vA_y\frac{\partial k}{\partial y} + wA_z\frac{\partial k}{\partial z}\right) = P_T + G_T + D_k - \varepsilon \quad (9)$$

$$\frac{\partial \varepsilon}{\partial t} + \frac{1}{V_F}\left(uA_x\frac{\partial \varepsilon}{\partial x} + vA_y\frac{\partial \varepsilon}{\partial y} + wA_z\frac{\partial \varepsilon}{\partial z}\right) = \frac{C_{1\varepsilon}\varepsilon}{k}\left(P_T + C_{3\varepsilon}G_T\right) + D_\varepsilon - C_{2\varepsilon}\frac{\varepsilon^2}{k} \quad (10)$$

where P_T is the turbulent kinematic energy production; G_T is the buoyancy production term; D_k and D_ε are the diffusion terms; and $C_{1\varepsilon}, C_{2\varepsilon}, C_{3\varepsilon}$ are constants.

2.2 Boundary Condition of Solitary Wave

This model uses the solitary wave source based on McCowan's theory [28]:

$$\eta = h\frac{N}{M}\frac{\sin\left[M\left(1+\frac{\eta}{h}\right)\right]}{\cos\left[M\left(1+\frac{\eta}{h}\right)\right] + \cosh\left[M\frac{x-ct}{h}\right]} \quad (11)$$

where η is the surface elevation, and h is the still water depth. Here, c is the wave velocity given by:

$$c = \bar{u} + c_0 \quad (12)$$

$$c_0 = \sqrt{g(h+H)} \quad (13)$$

where $\bar{u}$ is the current velocity, c_0 is the wave speed in still water, and H is the wave height.

The velocities are computed as:

$$u = \bar{u} + c_0 N \frac{1+\cos\left(\frac{Mz}{h}\right)\cosh\left(M\frac{x-ct}{h}\right)}{\left[\cos\left(\frac{Mz}{h}\right) + \cosh\left(M\frac{x-ct}{h}\right)\right]^2} \quad (14)$$

$$w = c_0 N \frac{\sin\left(\frac{Mz}{h}\right)\sinh\left(M\frac{x-ct}{h}\right)}{\left[\cos\left(\frac{Mz}{h}\right) + \cosh\left(M\frac{x-ct}{h}\right)\right]^2} \quad (15)$$

where N and M satisfy the two equations:

$$\frac{H}{h} = \frac{N}{M}\tan\left[\frac{1}{2}M\left(1+\frac{H}{h}\right)\right] \quad (16)$$

$$N = \frac{2}{3}\sin^2\left[M\left(1+\frac{2}{3}\frac{H}{h}\right)\right] \quad (17)$$

The Newton-Raphson method is applied for solving Eqs. (11-17) repeatedly. The initial values of M and N are $(3H/h)^{1/2}$ and $2H/h$, respectively. The initial value of the water surface elevation is given by

$$\eta_0 = H\,\mathrm{sech}^2\left[\sqrt{\frac{3}{4}\frac{H}{h}}\left(\frac{x-ct}{h}\right)\right] \quad (18)$$

3. RESULTS AND DISCUSSIONS

This section shows the verification of the numerical porous model. The first part of this section shows the stability of the solitary wave along the computational domain and the second part shows the energy dissipation effectiveness of the vertical porous breakwater for various cases.

3.1 Solitary Wave Propagation

For the simulation of waves overtopping vertical porous structures, a solitary wave is used as the initial condition and placed at the left boundary of the domain. The stability of a solitary wave is very important in numerical simulations. Figure 2 presents the surface profiles of the solitary wave at different positions along the computational domain. It shows that the shape and amplitude of the solitary wave are well conserved.

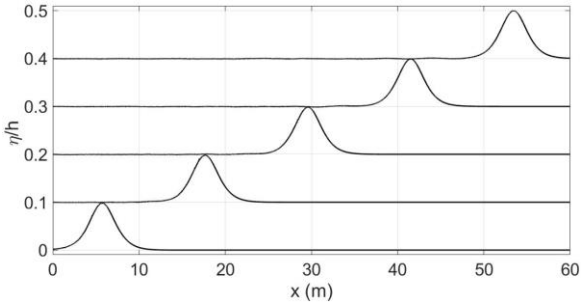

Fig.2 Solitary wave propagation along the computational domain.

3.2 Wave Overtopping of a Vertical Porous Breakwater

3.2.1 Model Setup

In this part, the solitary wave is applied as an initial condition to simulate waves interacting with the vertical porous structure for various cases. These cases include various breakwater widths and schematizations, porosities, initial wave heights, and water depths (Table 1).

The computational domain is shown in Fig.3.a with a uniform grid of $dx = dy = dz = 1$ cm. The laminar and turbulent coefficients of 10,000 and 80, respectively, are applied in these simulations. Two wave gauges are placed at 2 meters in front and 2 meters behind the vertical porous breakwater to record reflected and transmitted waves, respectively. A snapshot showing the flow field and the overtopping waves of the vertical porous breakwater is presented in Fig.3.b. Three types of the vertical porous breakwater are used for simulations. The first type is a single vertical porous breakwater (Fig.4.a), the second one (Fig.4.b) is a two-adjacent breakwater and the last one (Fig.4.c) has the same characteristics as the second one but with a gap in between two parallel breakwaters. As recommended, the porosity of the front breakwater should be greater than that of the rear one [19]. In this study the front breakwater has a width $B_1 = 0.3$ m filled with gravel diameter $d_1 = 8$ cm and porosity $\lambda_1 = 0.55$ while the rear one has a width $B_2 = 0.2$ m filled with gravel diameter $d_2 = 5$ cm and porosity $\lambda_2 = 0.45$, for the second type breakwater (Fig.4.b). The third type breakwater (Fig.4.c) has a gap of $B_1 = 0.3$ m between the front and rear breakwaters while the single type is simulated with 2 cases, $B = 0.2$ m and $B = 0.3$ m (Fig.4.a).

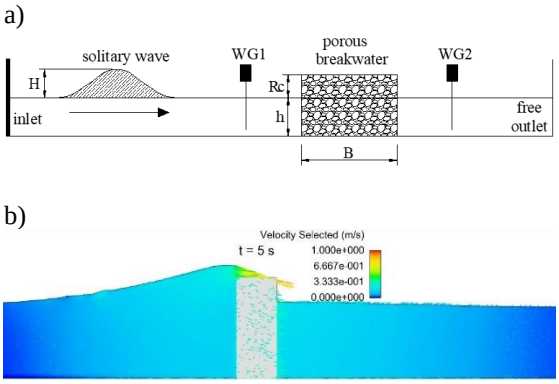

Fig. 3. Model domain: a) schematization; b) a snapshot of solitary wave overtopping of a vertical porous breakwater.

Table 1 Input parameters for the numerical model

Breakwater widths B (m)				Crest freeboard heights Rc (m)					
0.2	0.3	0.3 & 0.2	0.3, 0.3 & 0.2	-0.10	-0.05	0	0.05	0.10	0.15
Gravel diameter d (cm)		Porosities λ		Initial wave heights H (m)			Water depths h (m)		
5	8	0.45	0.50 0.55	0.06	0.09	0.12	0.35	0.40 0.45	0.50 0.55

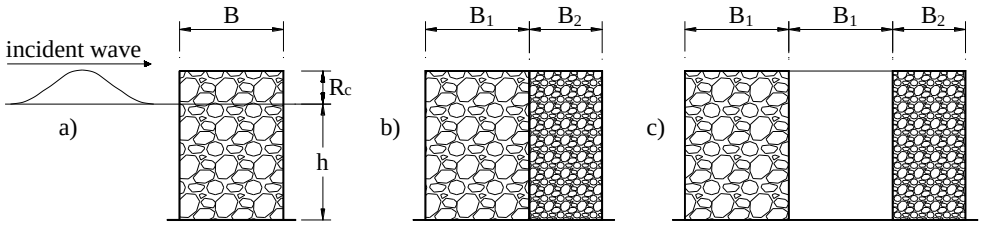

Fig. 4 Three types of porous breakwater scenarios: a) single breakwater, b) two adjacent breakwaters, c) parallel breakwaters with a gap.

3.2.2 Influence of Porous Breakwater Dimensions

This part carries out simulations for the first type of the breakwater scenario (Fig.4.a) with 2 breakwater width cases ($B = 0.2$ m and $B = 0.3$ m), gravel diameter $d = 5$ cm and porosity $\lambda = 0.5$. The incident solitary wave heights are $H = 0.06$ m, 0.09 m, and 0.12 m.

The energy dissipation coefficient is determined based on the energy balance of the incoming, reflecting, transmitting, and dissipating waves inside the structure. The energy balance around a porous structure obeys the law of energy conservation and is given by:

$$Ei = Er + Et + Ed \tag{19}$$

where Ei, Er, Et, and Ed are the energy of the incident, reflected, transmitted and dissipated waves, respectively. The energy balance can be written in terms of coefficients:

$$kd = \sqrt{1 - kt^2 - kr^2} \tag{20}$$

where kt, kr, and kd are transmission, reflection, and dissipation coefficients, respectively.

Figure 5 provides numerical results about the relation between the relative crest freeboard (Rc/H) and coefficients of transmission, reflection and dissipation. For submerged porous breakwater ($Rc/H < 0$), the breakwater widths do not significantly affect the wave transmission coefficient and the wave height behind the structure does not reduce much (i.e., less than 20%). In this case, waves behind the structure include waves passing through the porous body and waves propagate over the structure. It can be seen quite clearly that the deeper the crest freeboard inundation, the more insignificant the influence of the breakwater width on the transmission coefficient, the larger the incident wave height will give a larger wave height behind the porous structure but the coefficient kt is almost unchanged (i.e., $H = 0.06$, 0.09 , and 0.12 m then $kt = 0.83$, 0.83 , and 0.84 , respectively). The breakwater width is very small relative to the wavelength (a solitary wave is a long wave in shallow water), the width of the breakwater does not have much effect on the transmission coefficient for submerged breakwaters [29]. As the relative freeboard increases ($Rc/H > 0$), the influence of the breakwater width and the incident wave height on the transmission coefficient can be seen very clearly. When $Rc/H = 1.7$ (or $H = 0.06$ m), the kt for the 0.3 m width breakwater is about 83% of the kt for the 0.2 m width breakwater. This ratio is about 80% for $H = 0.09$ m and slightly reduce to 78% for $H = 0.12$ m. For all 3 cases of incident wave heights, the transmission coefficients become stable when the relative freeboard is greater than unity. This could be a good suggestion for physical experiments or cost savings in pilot projects. Most of the overtopping waves occur when the relative freeboard is from zero to unity.

When the relative freeboard is large enough (i.e., $Rc/H = 1 \div 2$), the transmission coefficient is almost constant because overtopping waves are negligible, the reflection coefficient slightly increases. The dissipation coefficient increases with the increase of the relative crest freeboard until $Rc/H < 1$, however, it decreases slightly for $Rc/H > 1$.

3.2.3 Influence of Breakwater Porosities

Three values of porosity used in this section ($\lambda = 0.45, 0.5, 0.55$) to evaluate the transmission coefficient are commonly applied in some numerical simulations of waves interacting with porous structures [4,6,9,30]. Figure 6 illustrates a similar trend as shown in the previous part. For low-crested breakwaters (i.e., $Rc/H \le 0$), the porosities do not have a significant effect on the transmission and reflection coefficients, especially when $Rc/H < -1$ since most of the waves propagate over the structure. For high-crested cases (i.e., $Rc/H > 0$), the porosities and incident wave heights give significant effects on reducing wave heights behind the breakwater. The dissipation and reflection coefficients show a similar trend with the increasing of the crest freeboard. Figure 6 clearly shows that when the porosity decreases, the transmission coefficient decreases.

3.2.4 Influence of Nonlinearities of Incoming Waves

Figure 7 shows the influence of the incident wave heights (the nonlinearity in the range of $H/h = 0.109 \div 0.343$) on the transmission, reflection and dissipation coefficients. The breakwater characteristics are breakwater width $B = 0.2$ m, the crest freeboard height $Rc = -0.1 \div 0.15$ m, porosity $\lambda = 0.5$, and gravel diameter $d = 5$ cm. It is shown that for submerged breakwater cases ($Rc \le 0$) or when crest freeboard heights are smaller than incident wave heights (i.e., $Rc = 0.05$ m), the transmission coefficient increases with higher incident waves since wave heights behind the porous breakwater are superposed by the transmission wave and overtopping wave. When the crest freeboard heights are greater than the incident wave heights ($Rc = 0.15$ m), the overtopping waves gradually reduce, waves behind the porous breakwater are sole transmission waves. Wave nonlinearities have a significant influence on the transmission coefficient, the more nonlinearity increases, the

more the transmission coefficient *kt* decreases and the reflection coefficient increases. This phenomenon has also been described in some other studies for simulations of solitary waves interacting with porous structures [3,4,6,30]. An interesting thing appears in Fig.7 when the trend of increasing or decreasing of *kt* is not evident for the crest freeboard height $Rc = 0.1$ m. For this case, the height of the crest freeboard is larger than wave heights $H = 0.06$ m & 0.09 m but smaller than $H = 0.12$ m. It can be seen that the transmission coefficients decrease gradually for the first two wave heights because when there is no or very little overtopping wave, the nonlinearity dominates. However, when the incident wave is higher than the crest freeboard, the transmission coefficient increases due to the dominance of the overtopping wave.

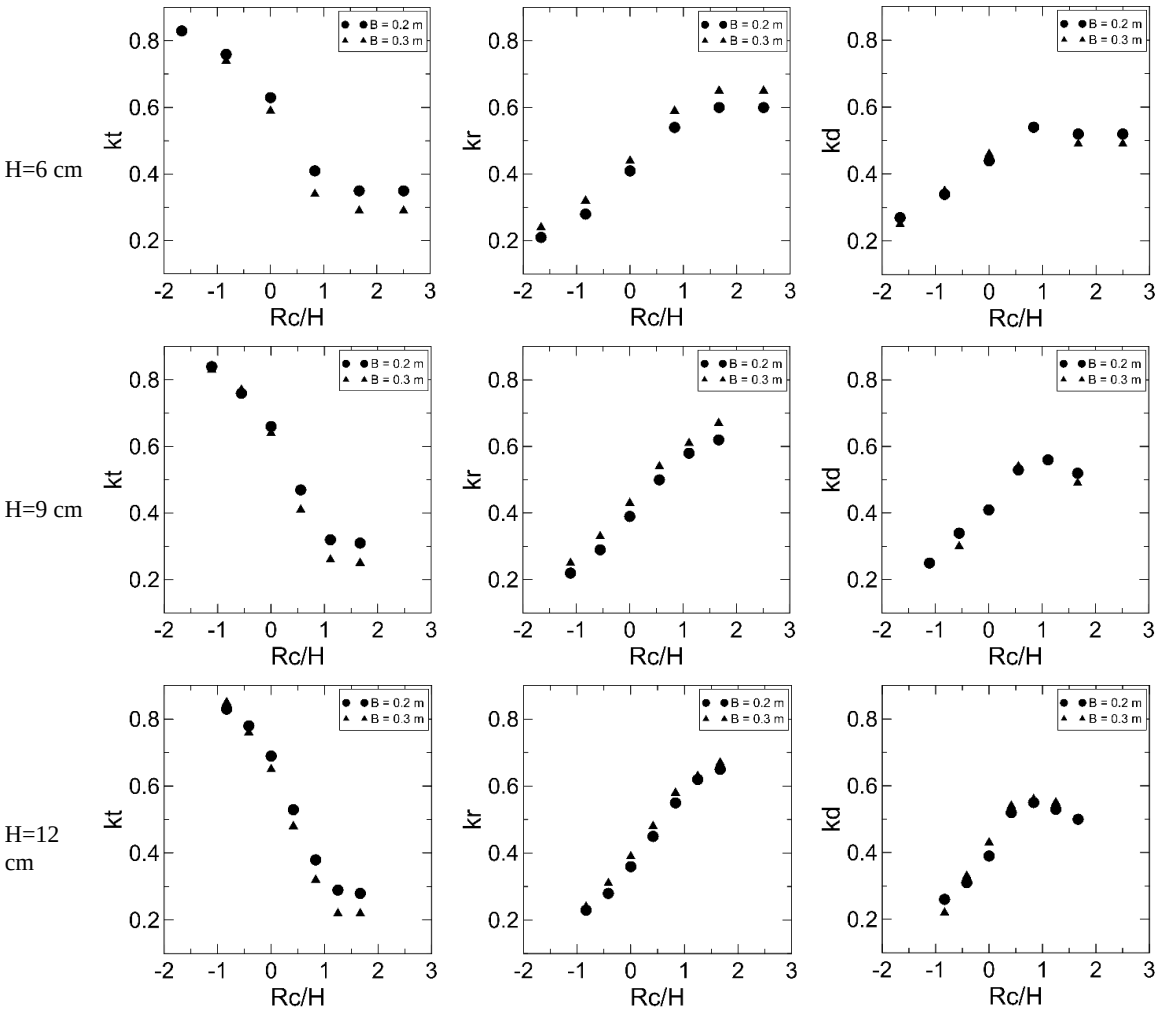

Fig.5 Influence of crest heights (*Rc*) to the transmission, reflection and dissipation coefficients.

3.2.5 Influence of the Breakwater Schematization

In the previous parts, a single porous breakwater is tested and shows its effectiveness in reducing wave energy. In this part, 2 cases of the porous breakwater schematization are tested (Fig.4.b, c). Figure 8.a gives numerical results for a two-adjacent breakwater case, the front breakwater (sea-ward) has a width $B_1 = 0.3$ m, the porosity $\lambda_1 = 0.55$, and the gravel diameter $d_1 = 8$ cm while the rear breakwater (land-ward) has a width $B_2 = 0.2$ m, the porosity $\lambda_2 = 0.45$ and the gravel diameter $d_2 = 5$ cm. Fig.8.b illustrates numerical results for parallel-breakwater with a gap case. The front and rear breakwaters are the same as the previous case however a gap $B_1 = 0.3$ m is set in between 2 breakwaters. In contrast to the cases described in the part 3.2.2 where the breakwater width does not significantly affect the wave propagation for the submerged breakwater, the breakwater width, in this case, shows a greater reduction in the *kt* coefficient,

and especially significantly decreases when the crest freeboard is greater than zero ($Rc > 0$).

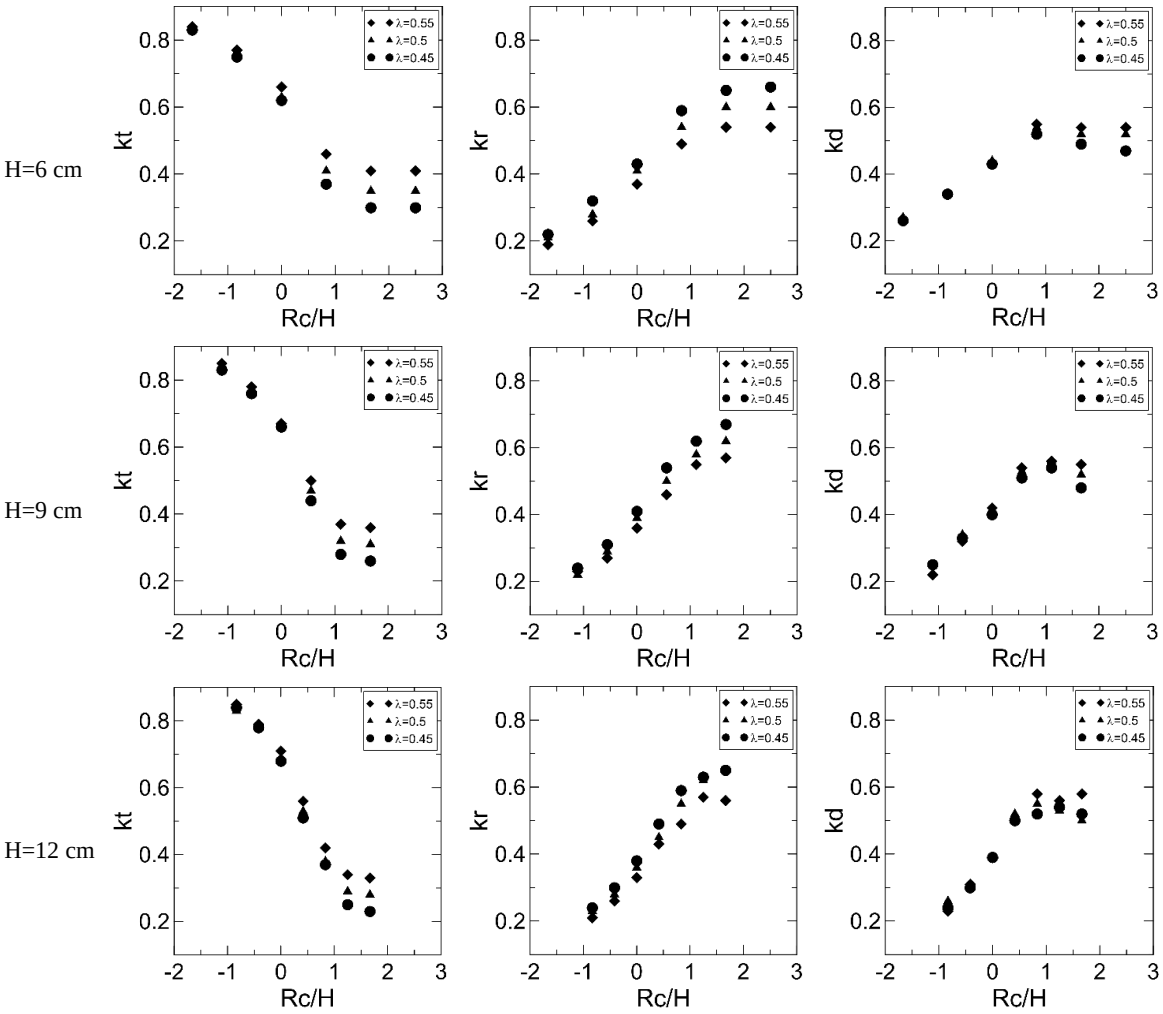

Fig.6 Influence of the porosities of the breakwater (λ) to the transmission, reflection and dissipation coefficients (breakwater width is $B = 0.2$ m).

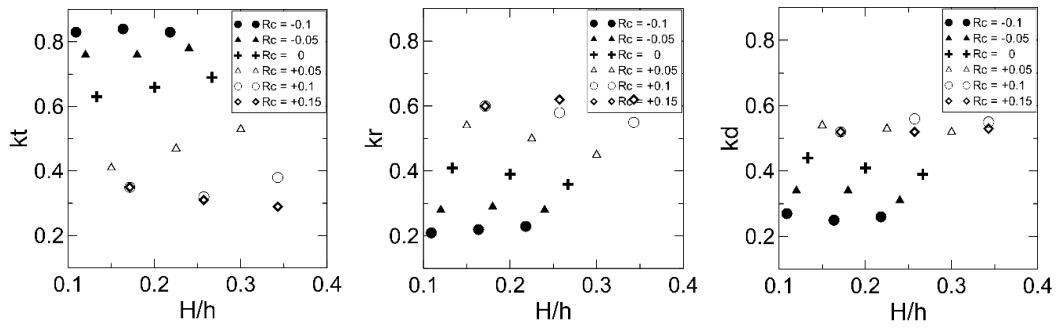

Fig. 7 Influence of the nonlinearities.

4. CONCLUSIONS

In this paper, a numerical model employing Navier-Stokes equations was introduced to simulate solitary waves overtopping a detached porous breakwater. The interaction of solitary waves with porous structures was conducted in several cases. We found that the breakwater width does not have a significant influence on the transmission coefficient for the simulation of long waves to a low-crested breakwater. The transmitted wave height is stable when the relative freeboard is greater than unity or the crest

freeboard height approximates the incoming wave height. This finding could be a good suggestion for physical experiments or cost savings in pilot projects being built in the lower Mekong Delta area. This study conducted numerical simulations of two more cases of the breakwater schematization (2 adjacent breakwaters and parallel breakwaters with a gap), which significantly reduce the wave heights behind the porous structure. However, these configurations may increase the construction costs and it is necessary to have more evaluation of the economic and technical efficiency of these types of detached porous breakwaters.

$H = 0.06\,\text{m}$ $H = 0.09\,\text{m}$ $H = 0.12\,\text{m}$

a) two adjacent breakwaters

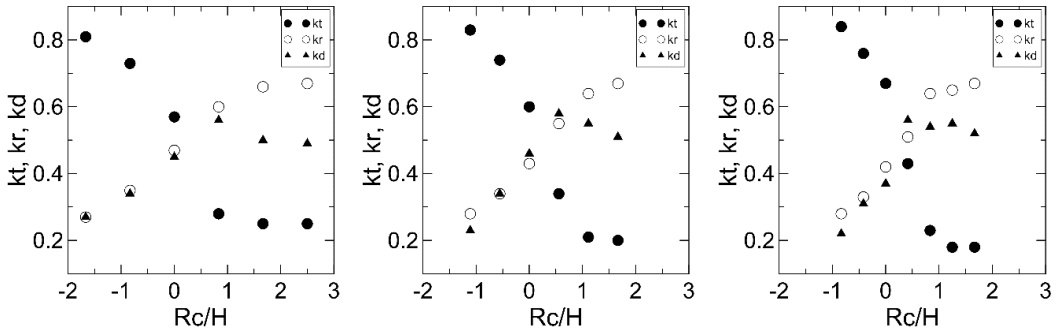

b) parallel breakwaters with a gap

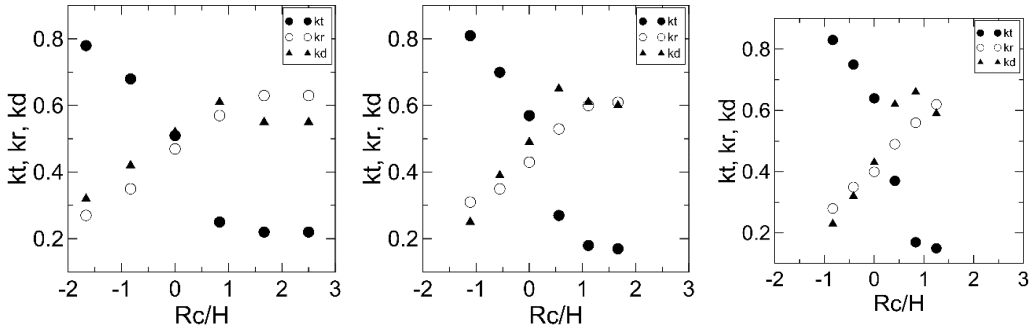

Fig. 8. Influence of the vertical porous breakwater schematizations.

5. ACKNOWLEDGMENTS

“ This research was funded by Vietnam National Foundation for Science and Technology Development (NAFOSTED) under grant number 107.03-2019.338”.

6. REFERENCES

[1] Cruz EC, Isobe M, Watanabe A., Boussinesq equations for wave transformation on porous beds, Coastal Engineering, Vol.30, Issue 1-2, 1997, pp. 125–56.

[2] Hsiao SC, Liu PLF, Chen Y., Nonlinear water waves propagating over a permeable bed, Proceedings of the Royal Society A: Mathematical, Physical and Engineering Sciences, Vol.458, No. 2022, 2002, pp. 1291–1322.

[3] Liu PLF, Wen J., Nonlinear diffusive surface waves in porous media, Journal of Fluid Mechanics, Vol.347, 1997, pp. 119–139.

[4] Vu VN, Lee C, Jung TH., Extended Boussinesq equations for waves in porous media, Coastal Engineering, Vol.139, 2018, pp. 85–97.

[5] Van Vu N, Trinh KT., Evaluation of the wave damping by a bamboo breakwater applying a porous media model, Lecture Notes in Civil Engineering, Vol.208, 2022, pp. 254-261.

[6] Vu VN, Lee C, Solitary wave interaction with porous structures, Procedia Engineering, Vol.116, 2015, pp. 834–841.

[7] Ma G, Shi F, Hsiao SC, Wu YT., Non-hydrostatic modeling of wave interactions with porous structures, Coastal Engineering, Vol.91, 2014, pp. 84–98.

[8] Zijlema M, Stelling G, Smit P., SWASH: An operational public domain code for simulating wave fields and rapidly varied flows in coastal

waters, Coastal Engineering, Vol.58, Issue 10, 2011, pp. 992–1012.
[9] del Jesus M, Lara JL, Losada IJ., Three-dimensional interaction of waves and porous coastal structures: Part I: Numerical model formulation, Coastal Engineering, Vol.64, 2012, pp. 57–72.
[10] Lara JL, del Jesus M, Losada IJ., Three-dimensional interaction of waves and porous coastal structures. Part II: Experimental validation, Coastal Engineering, Vol.64, 2012, pp. 26–46.
[11] Thieu Quang T, Mai Trong L., Monsoon wave transmission at bamboo fences protecting mangroves in the lower Mekong delta, Applied Ocean Research, Vol.101, 2020, pp. 1-14.
[12] Nguyet-Minh N., Cong-San, D., Van-Duong, D., Xuan-Tu, L., Nestmann, F., Zemann, M., Thai-Duong, V.H., Cong-Dan T., Evaluating the effectiveness of existing coastal protection measures in Mekong delta, Proceedings of the 10th International Conference on Asian and Pacific Coasts, Springer Nature Singapore Pte Ltd., 2019, pp. 1419–1429.
[13] Alongi DM., Mangrove forests: Resilience, protection from tsunamis, and responses to global climate change, Estuarine, Coastal and Shelf Science, Vol.76, 2008, pp. 1–13.
[14] Truong SH, Ye Q, Stive MJF., Estuarine Mangrove Squeeze in the Mekong Delta, Vietnam, Journal of Coastal Research,Vol.34, 2017, pp. 747–763.
[15] Dao T, Stive MJF, Hofland B, Mai T., Wave Damping due to Wooden Fences along Mangrove Coasts, Journal of Coastal Research, Vol34, 2018, pp. 1317–1327.
[16] Mai T, Dao T, Ngo A, Mai C., Porosity Effects on Wave Transmission Through a Bamboo Fence, Proceedings of the 10th International Conference on Asian and Pacific Coasts, Springer Nature Singapore Pte Ltd., 2019, pp. 1413-1418.
[17] Schmitt K, Albers T, Pham TT, Dinh SC., Site-specific and integrated adaptation to climate change in the coastal mangrove zone of Soc Trang Province, Viet Nam, Journal of Coastal Conservation. Vol.17, 2013, pp. 545–58.
[18] Tran VT, Nguyen HH, Pham DH, Nguyen DN, Nguyen TT, Hollow cylinder breakwater for dissipation of wave energy to protect the west coast of Ca Mau province in Vietnam, Lecture Notes in Civil Engineering, Vol.18, 2019, pp. 599-605.
[19] Liu Y, Li H., Analysis of wave performance through pile–rock breakwaters, Proceedings of the Institution of Mechanical Engineers, Part M: Journal of Engineering for the Maritime, Vol.228, Issue 3, 2014, pp.284-292.
[20] Herbich JB, Douglas B., Wave transmission through a double-row pile breakwater, Coastal Engineering Proceedings, No.21, 1988, pp. 165–165.
[21] Nguyen HH, Duong CM., Stability analysis of a double-row pile breakwater subjected to combined loading in Mekong Delta, Proceedings of the 10th International Conference on Asian and Pacific Coasts, 2019,pp. 1407–1411.
[22] Wu YT, Yeh CL, Hsiao SC., Three-dimensional numerical simulation on the interaction of solitary waves and porous breakwaters, Coastal Engineering, Vol.85, 2014, pp. 12–29.
[23] Zhao E, Dong Y, Tang Y, Xia X., Performance of submerged semi-circular breakwater under solitary wave in consideration of porous media, Ocean Engineering, Vol.223, 2021, pp. 1-19.
[24] Hirt C. W. and Nichols B. D., Volume of fluid (VOF) method for the dynamics of free boundaries, Journal of Computational Physics, Vol. 39, No. 1, 1981, pp. 201–225.
[25] Ergun S., Fluid flow through packed columns, Chemical Engineering Progress, Vol. 48, 1952, pp. 89–94.
[26] Harlow F. H., Turbulence Transport Equations, Physic Fluids, Vol. 10, No. 11, 1967, p. 2323–2332.
[27] Rodi W., Turbulence Models and Their Application in Hydraulics: A State of the Art Review. International Association for Hydraulic Research, Delft, The Netherlands, 1980.
[28] McCowan J., VII. On the solitary wave, The London, Edinburgh, and Dublin Philosophical Magazine and Journal of Science, Vol. 32, No. 194, 1891, pp. 45–58.
[29] van der Meer JW, Briganti R, Zanuttigh B, Wang B., Wave transmission and reflection at low-crested structures: Design formulae, oblique wave attack and spectral change, Coastal Engineering, Vol.52, 2005, pp. 915–929.
[30] Lynett PJ, Liu PL-F, Losada IJ, Vidal C., Solitary Wave Interaction with Porous Breakwaters, Journal of Waterway, Port, Coastal, and Ocean Engineering,Vol.126, 2000, pp. 314–322.